

Supporting Information for

Multiple Wavefront Shaping by Metasurface Based on Mixed

Random Antenna Groups

Dekel Veksler, Elhanan Maguid, Nir Shitrit, Dror Ozeri, Vladimir Kleiner, and Erez

Hasman *

Micro and Nanooptics Laboratory, Faculty of Mechanical Engineering, and Russell

Berrie Nanotechnology Institute, Technion – Israel Institute of Technology, Haifa

32000, Israel

*Correspondence should be addressed to: mehasman@technion.ac.il

1. Near-field radiation of an anisotropic nanoantenna

The coupling between a dipole radiation and surface plasmon waves was investigated in various aspects.^{S1-S3} Here, we focus on a dipole \mathbf{p} located in the origin and oriented parallel to the interface between dielectric ($z > 0$) and metal ($z < 0$) media, with dispersive dielectric constant functions $\varepsilon_1(\omega)$ and $\varepsilon_2(\omega)$, respectively. It was previously shown that for $r \gg k^{-1}$, the surface plasmon polariton (SPP) electric field generated by the dipole is^{S1}

$$\mathbf{E} \propto \frac{e^{ikr}}{\sqrt{kr}} \left(\hat{\mathbf{r}} - \frac{k}{\gamma_m} \hat{\mathbf{z}}_m \right) (\hat{\mathbf{r}} \cdot \mathbf{p}) e^{i\gamma_m |z|}. \quad (\text{S1})$$

Here, (z, r, φ) are cylindrical coordinates, $k(\omega) = \frac{\omega}{c} \sqrt{\frac{\varepsilon_1 \varepsilon_2}{\varepsilon_1 + \varepsilon_2}}$ is the SPP wave number,

where ω is the frequency and c is the speed of light, and γ_m satisfies the equation $\gamma_m^2 + k^2 = \varepsilon_m(\omega/c)^2$ with $m = 1$ and 2 for the dielectric and metal regions, wherein $\hat{\mathbf{z}}_m = \pm \hat{\mathbf{z}}$, respectively.

We express the dipole moment of an antenna in the x - y plane excited by a circularly polarized light via the polarizability tensor $\tilde{\alpha}$ as

$$\mathbf{p} = \tilde{\alpha} \cdot \mathbf{E}_{in} = \alpha E_0 \begin{pmatrix} 1 + \delta & 0 \\ 0 & 1 \end{pmatrix} \begin{pmatrix} \cos(\omega t) \\ -\sigma \sin(\omega t) \end{pmatrix}. \quad (\text{S2})$$

Here, $\delta = \alpha_x / \alpha_y - 1$, where α_x and α_y are the polarizabilities of the dipole in x and y directions, and α is a constant; E_0 is the incident light amplitude, and $\sigma_{\pm} = \pm 1$ is the photon spin corresponding to right and left circular polarizations, respectively. The nanoantenna parameter δ specifies its degree of isotropy, where for a spherical nanoantenna $\delta = 0$ and for a slender anisotropic nanoantenna (nanorod) $\delta \gg 1$.

Furthermore, the polarizability tensor of an anisotropic nanoantenna oriented at an angle θ is

$$\tilde{\alpha}_\theta = \alpha \begin{pmatrix} \cos \theta & -\sin \theta \\ \sin \theta & \cos \theta \end{pmatrix} \begin{pmatrix} 1 + \delta & 0 \\ 0 & 1 \end{pmatrix} \begin{pmatrix} \cos \theta & \sin \theta \\ -\sin \theta & \cos \theta \end{pmatrix}, \quad (\text{S3})$$

yielding that

$$\tilde{\alpha}_\theta = \alpha \begin{pmatrix} 1 + \delta/2 & 0 \\ 0 & 1 + \delta/2 \end{pmatrix} + \alpha \delta/2 \begin{pmatrix} \cos 2\theta & \sin 2\theta \\ \sin 2\theta & -\cos 2\theta \end{pmatrix}. \quad (\text{S4})$$

Thus, the dipole moment of the rotated antenna is

$$\mathbf{p}_\theta = E_0 \tilde{\alpha}_\theta \begin{pmatrix} \cos(\omega t) \\ -\sigma \sin(\omega t) \end{pmatrix}, \quad (\text{S5})$$

ushering in

$$\begin{aligned} \mathbf{p}_\theta = & \alpha E_0 \begin{pmatrix} 1 + \delta/2 & 0 \\ 0 & 1 + \delta/2 \end{pmatrix} \begin{pmatrix} \cos(\omega t) \\ -\sigma \sin(\omega t) \end{pmatrix} \\ & + \alpha \delta E_0/2 \begin{pmatrix} \cos 2\theta & -\sin 2\theta \\ \sin 2\theta & \cos 2\theta \end{pmatrix} \begin{pmatrix} \cos(\omega t) \\ \sigma \sin(\omega t) \end{pmatrix}. \end{aligned} \quad (\text{S6})$$

Note that the second term in eq S6 is manifested by an opposite spin state with regard to the incident field. This result originated from the second term of the polarizability tensor (eq S4) which is an improper rotation.

The dipole moment can be also expressed as

$$\mathbf{p}_\theta = \alpha E_0 \left((1 + \delta/2) \begin{pmatrix} \cos(\omega t) \\ -\sigma \sin(\omega t) \end{pmatrix} + \delta/2 \begin{pmatrix} \cos(2\sigma\theta + \omega t) \\ \sigma \sin(2\sigma\theta + \omega t) \end{pmatrix} \right), \quad (\text{S7})$$

or alternatively, in the phasor form as

$$\mathbf{p}_\theta = \left(A(\hat{\mathbf{x}} - i\sigma\hat{\mathbf{y}}) + B e^{-i2\sigma\theta}(\hat{\mathbf{x}} + i\sigma\hat{\mathbf{y}}) \right) p_0 e^{-i\omega t}, \quad (\text{S8})$$

where $\left| \frac{A}{B} \right| = \frac{1 + \delta/2}{\delta/2}$ and $p_0 = \alpha E_0$. This representation explicitly shows that the spin-

flip component is accompanied by a spin-dependent geometric phase term. By

substituting eq S8 into eq S1, we obtain that the SPP electric field generated by an oriented nanorod is

$$\mathbf{E} \propto \frac{e^{ikr}}{\sqrt{kr}} \left(\hat{\mathbf{r}} - \frac{k}{\gamma_m} \hat{\mathbf{z}}_m \right) e^{i\gamma_m |z|} \left(A \left(\frac{x - i\sigma y}{\sqrt{x^2 + y^2}} \right) + B e^{-i2\sigma\theta} \left(\frac{x + i\sigma y}{\sqrt{x^2 + y^2}} \right) \right) p_0 e^{-i\omega t}, \quad (\text{S9})$$

or in a more simplified manner as

$$\mathbf{E} \propto \frac{e^{ikr}}{\sqrt{kr}} \left(\hat{\mathbf{r}} - \frac{k}{\gamma_m} \hat{\mathbf{z}}_m \right) e^{i\gamma_m |z|} \left(A e^{-i\sigma\varphi} + B e^{i(\sigma\varphi - 2\sigma\theta)} \right) p_0 e^{-i\omega t}. \quad (\text{S10})$$

Note that the resulting field is composed of a propagating SPP wave acquiring an orbital angular momentum (AM) that is equal to the incident spin AM, and a secondary SPP wave with an opposite orbital AM and a spin-dependent geometric phase

$$E \propto \frac{e^{ikr}}{\sqrt{kr}} \left(A e^{-i\sigma\varphi} + B e^{i(\sigma\varphi - 2\sigma\theta)} \right). \quad (\text{S11})$$

For extremely anisotropic nanoantenna with $\delta \gg 1$ (i.e., $A = B$) we obtain

$$E \propto \frac{e^{ikr}}{\sqrt{kr}} \left(e^{-i\sigma\varphi} + e^{i(\sigma\varphi - 2\sigma\theta)} \right). \quad (\text{S12})$$

The presented analytical calculation was confirmed by a finite difference time domain (FDTD) simulation (RSoft FullWAVE) of the electromagnetic near-field distribution. We simulated a propagating SPP wave generated by a single 40-by-500-nm² anisotropic void antenna imbedded to a depth of 100 nm into a 200 nm thick gold film. The nanoantenna was normally illuminated with a circularly polarized light at a wavelength of 750 nm. We present the normal E_z field which is the dominant component in the electromagnetic near-field distribution. The analytical calculation (Figure S1c,d) exhibits good agreement with the FDTD simulation (Figure S1a,b).

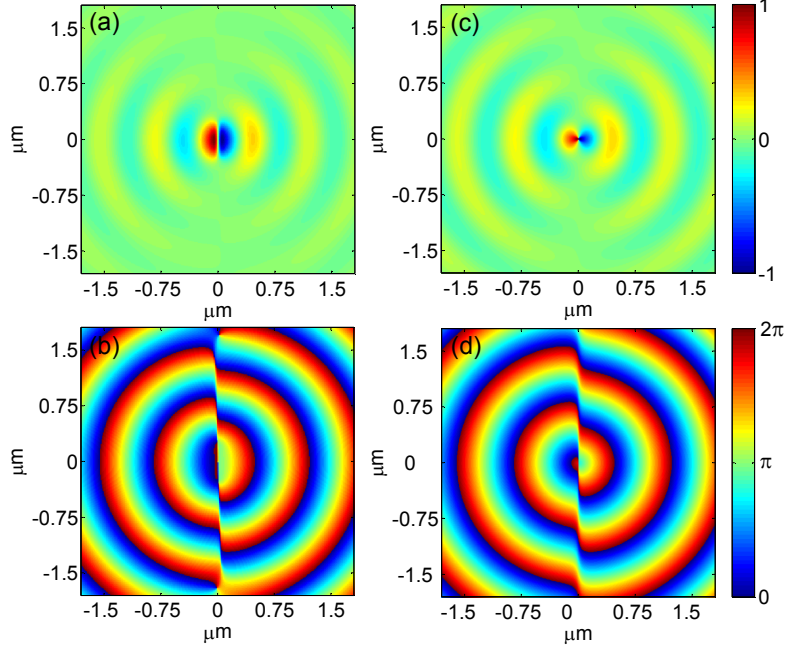


Figure S1. Near-field distribution of a plasmonic anisotropic nanoantenna. (a,b) FDTD simulation of the real part and the phase of the E_z field, respectively. (c,d) Analytical calculation of the real part and the phase of E_z , respectively, according to eq S11, with $A/B = 1.05$.

2. Comparison between periodic and random sampling

We performed a numerical calculation to investigate the open channels in periodic and disordered metasurfaces, in the regime that the characteristic distance between nanoantennas in each channel d is larger than the wavelength λ . The disordered gradient metasurface (DGM) was designed to open a single spin-dependent channel along the x axis at a wavelength of 765 nm, under normal incidence. On the other hand, in the periodic metasurface with a similar orientation function of nanoantennas (eq 2), the locations are set according to the local periodicity of d . The calculation, based on the interference of anisotropic antenna fields, shows that a single channel is opened in the DGM (Figure S2c,d), whereas in the periodic metasurface additional

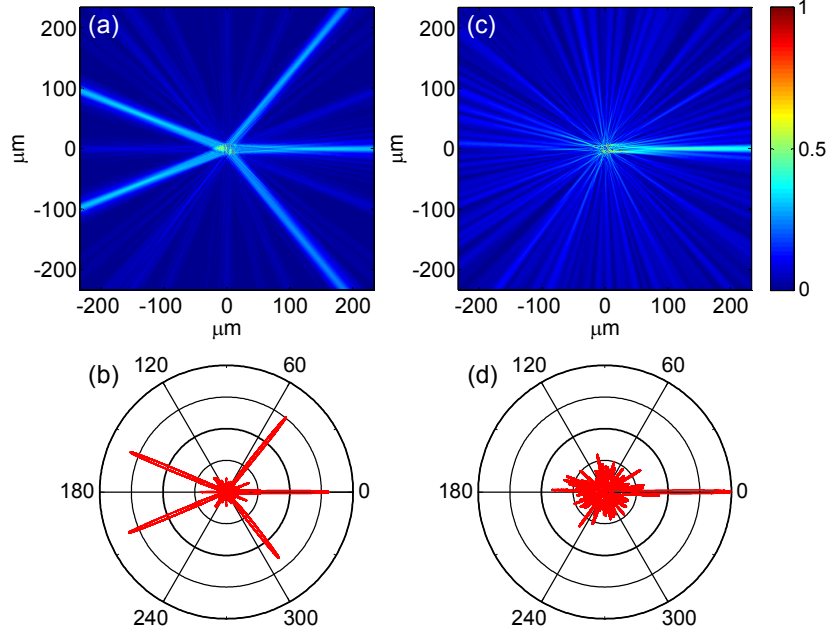


Figure S2. Open channels in periodic and disordered metasurfaces with a characteristic distance larger than the wavelength. (a,b) Calculated intensity distribution and azimuthal cross section of the channels opened by a periodic square lattice, respectively, with a local periodicity of $d = 2.6\lambda$. In the polar representation, the azimuthal angle is given in degrees and the intensity is on a linear scale. (c,d) Calculated intensity distribution and azimuthal cross section of the channel opened by a disordered metasurface, respectively, with a characteristic distance between nanoantennas of $d = 2.6\lambda$. The calculations were performed with σ_+ excitation.

by-product channels arise (Figure S2a,b). This result manifests the advantage of DGMs compared to ordered systems as they enable a sampling of the desired phase profile with $d \gg \lambda$, which is essential for opening multiple channels under the geometric limitation of $N_c^{(g)} \propto d^2$.

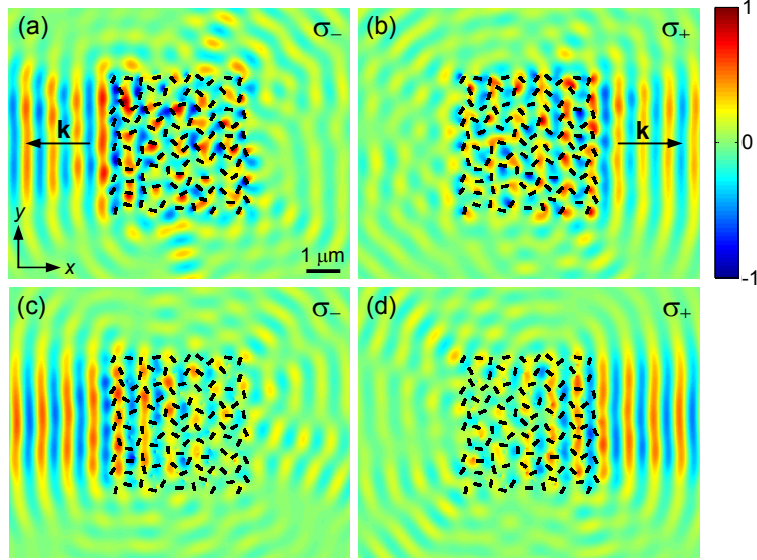


Figure S3. Calculations of a near-field open channel in a disordered metasurface. (a,b) FDTD simulations of the real part of the E_z field for σ_- and σ_+ excitations, respectively. The randomly distributed nanoantennas with designed orientations in the 4-by-4- μm^2 array are depicted by the rectangles. (c,d) Interference-based calculations of the real part of the SPP field for σ_- and σ_+ excitations, respectively.

3. Calculations of a plasmonic disordered gradient metasurface

We calculated the electromagnetic near-field distribution of a DGM by a FDTD simulation to confirm the validity of the analytical results, obtained by the superposition of SPP scattered fields from anisotropic antennas with designed orientations. The randomly distributed nanoantennas were oriented according to eq 2 for opening a single spin-dependent channel along the x axis at an incident wavelength of 750 nm (see Figure S3). The 80-by-220-nm² void antennas were imbedded to a depth of 100 nm into a 200 nm thick gold film. The normal E_z fields for normally incident right and left circularly polarized light were detected at 50 nm above the gold-air interface. The FDTD simulations of the spin-controlled open

channels are shown in Figure S3b,a, where propagating SPP jets in the $\pm x$ directions corresponds to an incident optical spin of σ_{\pm} , respectively, with good agreement to the analytical calculations shown in Figure S3d,c.

4. Efficiency of surface plasmon polariton excitation by disordered gradient metasurface

We performed FDTD simulations to study the light-to-SPPs coupling efficiency of a single open channel periodic and DGMs normally illuminated by circularly polarized light. The coupling efficiency was evaluated by examining the antiresonance dips in the reflection spectrum as a result of the absorption to SPP modes. The simulated gradient metasurfaces consist of 80-by-220-nm² nanoantennas etched to a depth of 150 nm into a thick gold film. Two DGMs were designed to open a single near-field channel with SPP wavelengths of 740 and 800 nm. The simulated reflection spectra of these DGMs are manifested by antiresonance dips corresponding to the designed SPP wavelengths (Figure S4). Moreover, the DGMs exhibit coupling efficiencies of $\approx 15\%$ and 7% at the wavelengths of 740 and 800 nm, respectively. The dependence of the DGM coupling efficiency in the wavelength arises from the wavelength-dependent variation of the local polarizability of a single anisotropic nanoantenna; hence, metasurfaces with different resonant wavelengths exhibit different coupling efficiencies. Note that the reported efficiency corresponds to a single channel DGM, while for a multichannel DGM, with similar total number of antennas, the efficiency decreases by the factor $1/N_c^2$, where N_c is the number of open channels (see Figure 2e). For comparison, periodic gradient metasurfaces with same resonances and density of nanoantennas were also simulated (Figure S4). The reflection spectra of the

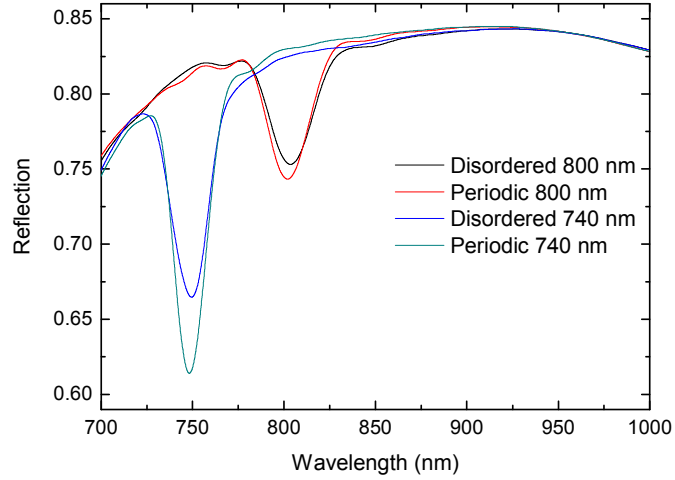


Figure S4. Simulated reflection spectra of a single channel gradient metasurfaces.

The simulated periodic and DGMs are $20\text{-by-}2\text{-}\mu\text{m}^2$ nanoantenna arrays.

periodic metasurfaces are similar to the corresponding DGMs and their coupling efficiencies are slightly higher ($\approx 2\% - 5\%$) than the efficiencies of the DGMs.

5. Spectral measurement of a disordered gradient metasurface with multiple near-field channels

The transmission spectrum of a DGM with mixed antenna groups bears the signature of the operating wavelengths of the near-field open channels as a result of the SPP excitation. A DGM consisting of rectangular void nanoantennas etched into a gold film was designed to open three channels in the near field at SPP wavelengths of 690, 760, and 830 nm. Note that this wavelength range is within the broad polarization-based spectral response of the anisotropic nanoantenna. This DGM was normally illuminated by a collimated white light beam (Quartz Tungsten Halogen lamp) and the transmission spectrum was measured in the far field. The presented transmission spectrum of the multichannel DGM (Figure S5) was normalized to the transmission

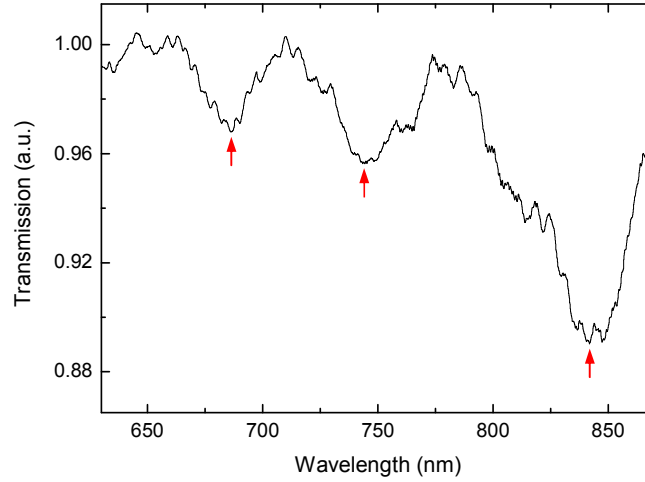


Figure S5. Transmission spectrum of a three open channel disordered gradient metasurface. The arrows correspond to the designed absorption lines, i.e., SPP wavelengths, of the near-field open channels.

spectrum of a randomly oriented nanoantenna metasurface. This spectrum is manifested by antiresonances in the corresponding SPP wavelengths as a result of the absorption to SPP modes, where the experimentally observed SPP wavelengths exhibit good agreement with the designed wavelengths. The illuminated free-space wavelengths of the different open channels are calculated then from the SPP dispersion at the gold-air interface.

6. Crosstalk measurements in the near field

In a multichannel system, the crosstalk between channels is a critical issue that may limit the number of open channels as a result of an undesired effect that one channel creates in the other channels. As part of the characterization of the DGM information capacity, we study the crosstalk influence by opening channels with similar directionality and different operating wavelengths. In a DGM designed to open two

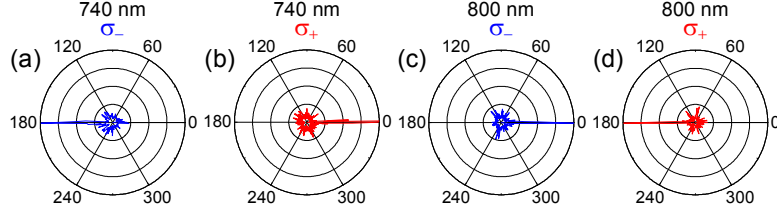


Figure S6. Crosstalk measurements of a multichannel disordered gradient metasurface. (a-d) Spin-controlled near-field open channels with similar directionality and different operating wavelengths. The measured intensities along the slit show the open channels for σ_- and σ_+ excitations, at wavelengths of 740 (panels a and b) and 800 nm (panels c and d), respectively.

spin-dependent channels in the near field, the σ_+ channels excite SPPs propagating in 0° and 180° directions for 740 and 800 nm, respectively (Figure S6b,d), whereas σ_- channels are oppositely directed (Figure S6a,c). The measured azimuthal cross sections show that the crosstalk between the two open channels is rather weak (see Figure S6).

7. Signal-to-noise ratio calculation

The increase in the number of open channels N_c in a DGM is accompanied by a reduction of the signal-to-noise ratio (SNR) of each channel. We characterized this dependence by a numerical calculation based on the interference model. For the SNR calculation, we considered two types of structures: single- and multiple-channel DGMs, wherein the total number of antennas N_t is constant. In the multiple-channel DGM, the total number of antennas was divided into mixed groups, so one group opens a channel along the x axis at an incident wavelength of 765 nm, whereas all other channels are opened in different directions and operate at a wavelength of 1.3

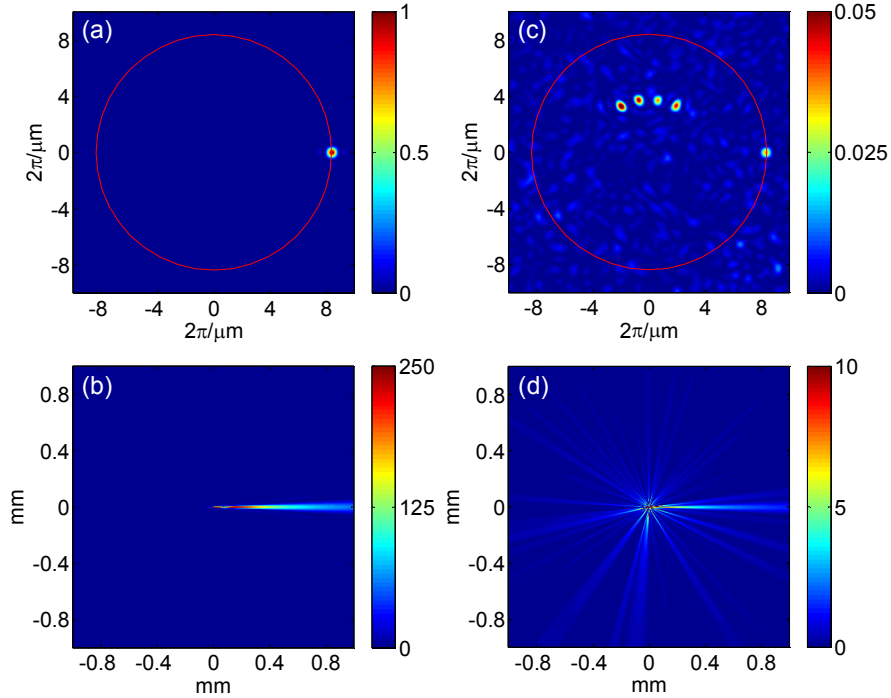


Figure S7. SNR calculation. (a,b) Momentum space and real space intensity calculations of a single open channel metasurface, respectively. The red circle represents the k_{SPP} circle corresponding to a SPP wavelength of 750 nm. (c,d) Momentum space and real space intensity calculations of a metasurface with five open channels, respectively. The calculations were performed with σ_+ excitation.

μm (Figure S7c). The channels were separated in the reciprocal space to eliminate the crosstalk between channels. We performed a calculation of the intensity distributions of a single (Figure S7b) and five open channels (Figure S7d) for σ_+ normal-incidence illumination, at the wavelength of 765 nm. The speckle pattern is clearly seen in the calculations as a noise source. The noise was calculated via the standard deviation of the signal intensity in a segment in the real space, where there is no open channel. From this procedure we obtained that the intensity of each channel scales as $(N_i / N_c)^2$ (see Figure 2e and note the different intensity scales in Figure S7b,d), the

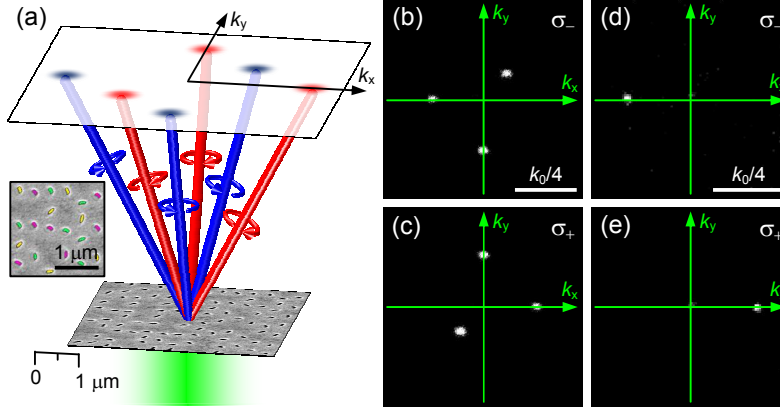


Figure S8. Free-space interconnects of plane waves based on a disordered gradient metasurface. (a) Schematic of spin-controlled far-field open channels by a disordered metasurface. The inset shows the mixed antenna groups, where each color corresponds to a different channel. (b,c) Spin-flip momentum deviations of 3 open channels for σ_- and σ_+ spin states of the scattered light, respectively, at a wavelength of 740 nm. The polarization state is resolved with the use of a circular polarization analyzer (a quarter-wave plate followed by a linear polarizer). (d,e) Spin-flip momentum deviations of a single open channel with $d \approx 2\lambda \approx 1.5\mu\text{m}$ for σ_- and σ_+ scattered spin states, respectively.

noise intensity scales as N_i , and hence, the SNR is proportional to N_i/N_c^2 (see Figure 2f).

8. Multiple far-field open channels of plane waves

DGMs can also open channels in the far field providing the route for free-space interconnects. We demonstrated a general fan-out interconnect of plane waves based on an ultrathin spin-optical DGM (Figure S8a). By orientating the nanoantennas of each channel according to eq 2, a spin-controlled free-space channel with a transverse

momentum shift k_g is opened. The corresponding scattered component undergoes deflection at an angle of $\arcsin(\sigma k_g / k_0)$, and spin flip to an opposite spin state with regard to the incident beam with the wave number k_0 . The peculiarity of the disordered approach enabling to open channels with $d > \lambda/2$ was presented via a metasurface wherein $d \approx 2\lambda$ (Figure S8d,e). We also observed 3x2 spin-dependent channels of plane waves in desired directions (Figure S8b,c), thereby introducing the ability to utilize light control by multifunctional DGMs for interconnects.

9. Achromatic nature of far-field open channels

Geometric metasurfaces based on the geometric phase can operate over a broad wavelength range, where the generation of far-field open channels does not require a matching to the SPP momentum. The peculiarity of the geometric phase lies in its geometric nature; unlike diffractive and refractive elements, it does not arise from optical path differences but from a space-variant manipulation of the light polarization state. The geometric phase of $2\sigma\theta(x,y)$ generated by a gradient metasurface with space-variant anisotropic nanoantennas depends only on the incident circular polarization σ and on the local orientation angle θ . Hence, this phase is independent of the wavelength. Practically, geometric metasurfaces based on the geometric phase operate as achromatic devices within the broad polarization-based spectral response of the anisotropic nanoantenna.

We study the achromatic nature of DGMs by observing the far-field open channels at a broad wavelength range. By orientating the nanoantennas of each channel according to $2\theta(x,y) = \alpha x + l\varphi$, a spin-controlled free-space channel with an independent design of the propagation direction and the orbital AM is opened, where

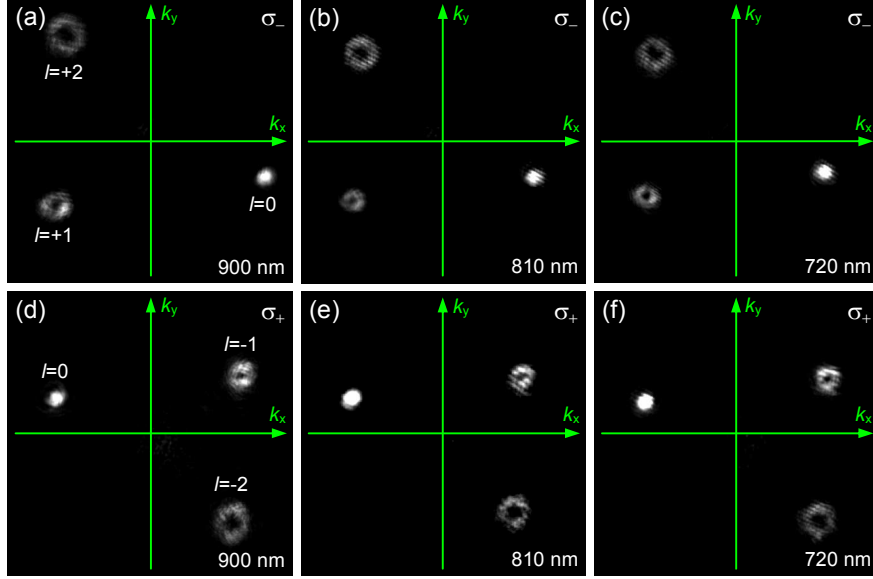


Figure S9. Achromatic nature of far-field open channels. (a-f) Spin-flip momentum deviations of three open channels with different orbital angular momenta for σ_- and σ_+ spin states of the scattered light, at varying illuminating wavelengths of 720 (panels c and f), 810 (panels b and e) and 900 nm (panels a and d), respectively. The polarization state is resolved with the use of a circular polarization analyzer (a quarter-wave plate followed by a linear polarizer).

the integer number l is the topological charge and φ is the azimuthal angle. The corresponding scattered component carries an orbital AM of σl and undergoes deflection at an angle of $\arcsin(\sigma\alpha/k_0)$, where $k_0 = 2\pi/\lambda$ and σ are the wave number and the spin state of the incident beam; moreover, the scattered component is manifested by a spin flip to an opposite spin state with regard to the incident beam. We measured the spin-flip components of the 3x2 spin-dependent channels at different operating wavelengths (Figure S9). The observed far-field intensity distributions are similar at all wavelengths, where the deflection angles of the channels, corresponding to the momentum deviations, increase with the wavelength

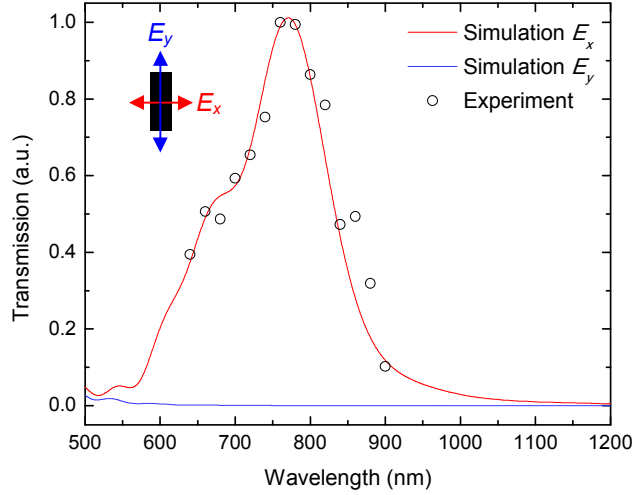


Figure S10. Polarization-based transmission spectra of a single anisotropic nanoantenna. Red and blue lines correspond to FDTD simulations of linear polarization excitations parallel and perpendicular to the minor axis of the 80-by-220-nm² void nanoantenna, respectively. The experimental points were obtained by measuring the intensity of a far-field open channel at different wavelengths.

according to $\arcsin(\sigma\alpha\lambda/2\pi)$ (see Figure S9). Hence, DGMs generating far-field open channels that do not require a matching to the SPP momentum exhibit wavelength-independent operation.

10. Spectral properties of a single anisotropic void antenna

In order to maximize the intensity of the open channels, the dimensions of the unit cell of the DGM, i.e., an anisotropic rectangular void nanoantenna, should be optimized to exhibit high polarization anisotropy in the spectral region of interest. We studied and optimized the localized mode resonance of the anisotropic nanoantenna by FDTD simulations. A single 80-by-220-nm² void antenna imbedded to a depth of 100 nm into a 200 nm thick gold film was considered and we simulated the

transmission spectrum of such an anisotropic nanoantenna for two orthogonal linear polarization excitations parallel and perpendicular to its minor axis (Figure S10). High polarization anisotropy is clearly observed between the two linear polarization excitations resulting from the anisotropy of the nanoantenna. The localized mode resonance of the antenna is obtained at a wavelength of 770 nm with the linear polarization excitation parallel to its minor axis. We experimentally characterized the transmission spectrum of a single nanoantenna by measuring the far-field intensity of a plane wave open channel generated by a DGM, at different illuminating wavelengths. The obtained experimental points (Figure S10) concur with the simulated transmission spectrum and verify the polarization-based response of the anisotropic nanoantenna.

References

- (S1) Archambault, A.; Teperik, T. V.; Marquier, F.; Greffet, J. J. Surface plasmon Fourier optics. *Phys. Rev. B* **2009**, *79*, 195414.
- (S2) Hecht, B.; Bielefeldt, H.; Novotny, L.; Inouye, Y.; Pohl, D. W. Local excitation, scattering, and interference of surface plasmons. *Phys. Rev. Lett.* **1996**, *77*, 1889-1892.
- (S3) Novotny, L.; Hecht, B. *Principles of Nano-Optics*; Cambridge Univ. Press: Cambridge, 2006.